Chapter 3

Unscented Kalman Filter for State and Parameter Estimation in Vehicle Dynamics

Mark Wielitzka, Alexander Busch,
Matthias Dagen and Tobias Ortmaier

Additional information is available at the end of the chapter

http://dx.doi.org/10.5772/intechopen.71900

Abstract

Automotive research and development passed through a vast evolution during past decades. Many passive and active driver assistance systems were developed, increasing the passengers' safety and comfort. This ongoing process is a main focus in current research and offers great potential for further systems, especially focusing on the task of autonomous and cooperative driving in the future. For that reason, information about the current stability in terms of dynamic behavior and vehicle environment are necessary for the systems to perform properly. Thus, model-based online state and parameter estimation have become important throughout the last years using a detailed vehicle model and standard sensors, gathering this information. In this chapter, state and parameter estimation in vehicle dynamics utilizing the unscented Kalman filter is presented. The estimation runs in real time based on a detailed vehicle model and standard measurements taken within the car. The results are validated using a Volkswagen Golf GTE Plug-In Hybrid for various dynamic test maneuvers and a Genesys Automotive Dynamic Motion Analyzer (ADMA) measurement unit for high-precision measurements of the vehicle's states. Online parameter estimation is shown for friction coefficient estimation performing maneuvers on different road surfaces.

Keywords: vehicle dynamics, state estimation, parameter estimation, unscented Kalman filter, dead-time compensation

1. Introduction

In the past decades, enormous developments in automotive research were achieved. Since the beginning of the twentieth century, a consistent search for solutions increasing vehicle's safety and comfort took place. Starting with passive safety systems in the early twentieth century, e.g., airbag, safety belt, and deformable zone, a vast improvement of the passenger's safety was accomplished. These systems reduce passenger injuries and or even death due to accidents.

Later, starting in the 1960th and 1970th active safety systems or advanced driver assistance systems (ADAS), preventing the vehicle from accidents by actively influencing the vehicle was developed. First implementations were traction control (TCS) and antilock braking systems (ABS), stabilizing the vehicle during longitudinal dynamic maneuvers. In 1995, the superordinate electronic stability control (ESC) was developed, combining stabilization during longitudinal and lateral dynamic maneuvers. Because of its success, ESC is mandatory in modern vehicles in Europe since the end of 2014. Other ADAS, e.g., adaptive cruise control (ACC), autonomous emergency braking (AEB), or lane detection system, have been developed in the meantime, further increasing safety and comfort. Future trends show an enormous potential for advanced systems, finally leading to the objective of autonomous and cooperative driving.

Many of these ADAS rely on parametric models, describing and predicting the vehicle's (future) behavior. Especially information about the vehicle's stability, characterized by dynamic states, is necessary. Furthermore, information about the vehicle's environment, e.g., by changing weather conditions and therefore changing friction conditions may influence the systems' performance drastically. Thus, online estimation of the vehicle's stability in terms of its dynamic behavior and online estimation of influential parameters, such as the friction coefficient, are challenging fields in modern automotive research.

Many methods for state estimation use simple models of vehicle dynamics to reduce the computational effort, e.g., considering a linear bicycle model [1–3] or a linear planar two-track model [4]. A further detailed description of the forces acting on the vehicle's tire is developed in Ref. [5] and utilized in Ref. [6]. A more detailed model, considering roll dynamics (cf. **Figure 1**), is utilized in [7, 8].

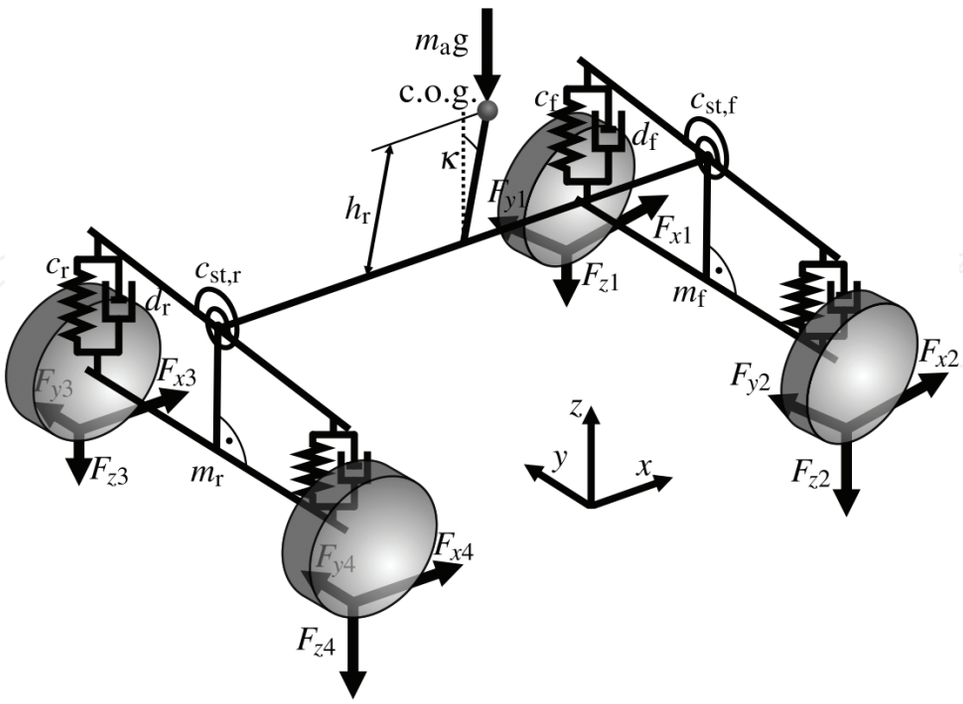

Figure 1. Two-track model including roll dynamics of a vehicle performing a left turn.

Similarly, various methods considering the estimation algorithm are utilized. For linear models, the Kalman filter serves as an optimal filter. Considering nonlinear models, Kalman filter derivatives, such as extended and unscented Kalman filters (EKF/UKF), are used. The EKF is used for tire road force and sideslip angle estimation in Ref. [9] and for sideslip angle estimation of low friction roads in Ref. [6]. The UKF for vehicle state estimation is presented in [7, 8].

Simultaneous state and parameter estimation with dual extended Kalman filter is presented in Ref. [10], estimating the vehicle mass and moment of inertia around the vertical axis. The same parameters are estimated in Ref. [11] using a joint UKF. Friction coefficient estimation using a joint UKF is realized in [12–14].

In this chapter, state estimation in vehicle dynamics utilizing an UKF is presented. The estimation is based on measurements taken with standard sensors, which are implemented in modern vehicles. Therefore, a nonlinear process and measurement model are introduced. Furthermore, dead times, due to CAN communication, are considered and compensated using model-based methods. Additionally, simultaneous state and parameter estimation considering the friction coefficient between tires and road is presented. All methods are validated online using a Volkswagen Golf GTE Plug-In Hybrid as the test vehicle, equipped with a Genesys ADMA inertial platform for precise reference measurements. The friction coefficient estimation is validated on a test track with two different surfaces.

The chapter is organized as follows: in Section 2, the nonlinear process and measurement models of the vehicle's longitudinal and lateral dynamics are introduced. Based on this, Section 3 addresses the state and parameter estimation utilizing the unscented Kalman filter. Furthermore, dead-time compensation and bounded parameter estimation are introduced. In Section 4, the estimation results, using this method, are presented. Thus, measurements taken on a test vehicle using a precise initial measurement unit are presented and discussed. The chapter is recapped with a Conclusion in Section 5.

2. Modeling

In this section, a detailed parametric model of the vehicle's dynamics is presented. Deriving this model for online application, a trade-off between accuracy and computational effort has to be faced. Starting from the contact patch of tires and road as a predominant source of forces acting on the vehicle, the full dynamics of the vehicle will be derived. Furthermore, a measurement model describing certain measurements, representing the vehicle's dynamics taken with standard sensors is presented. The resulting models form the basis for the later state and parameter estimation algorithm using the UKF.

2.1. Tire model

First, the vehicle's tires are considered, representing the contact patch between vehicle and road, consequently providing forces substantially influencing the vehicle's dynamics. These forces arise due to differences in relative motion between tire and road and therefore lead to a

deformation of the tire due to friction, described by the friction coefficient μ. These differences in velocity can be expressed as tire slip

$$\lambda = \frac{\omega_t r_t - v_{t,x}}{\max(\omega_t r_t, v_{t,x})}, \tag{1}$$

for longitudinal and tire sideslip angle

$$\alpha = \delta_t - \arctan\left(\frac{v_{t,y}}{v_{t,x}}\right), \tag{2}$$

for lateral motion, respectively, where ω_t represents the rotational velocity of the tire, δ_t is the tire steering angle, $v_{t,x,y}$ is the components of the wheel's velocity v_t, and r_t is the effective tire radius, which is considered a constant. The tire steering angle results from the steering wheel angle δ as $\delta = i_{st}\delta_t$, with the assumption of constant steering transition i_{st}. Coming from the well-known Coulomb friction $F_{fric} = \mu F_z$, with normal force F_z, the associated stationary tire forces in longitudinal and lateral direction, F_x^S and F_y^S, are functions of the tire slip and sideslip angle, respectively, given as

$$F_x^S = f_x(\lambda, \mu_{max}, F_z)h(F_y), \tag{3}$$

$$F_y^S = f_y(\alpha, \mu_{max}, F_z)h(F_x), \tag{4}$$

assuming identical maximum friction coefficient for longitudinal and lateral forces. The nonlinear functions $f_{x,y}$ represent the (side)slip dependency of the tire forces by the magic formula tire model described by

$$f_{x,y}(\chi, \mu_{max}, F_z) = D \sin\left(C\arctan\left(B\frac{\chi}{\mu_{max}} - E\left(B\frac{\chi}{\mu_{max}} - \arctan\left(B\frac{\chi}{\mu_{max}}\right)\right)\right)\right), \tag{5}$$

with individual parameters for longitudinal and lateral dynamics $D = \mu_{max}F_z$, $B = C_F/CD$, and $C_F = c_1 \sin(2\arctan(F_z/c_2))$, while χ represents the slip λ or sideslip α [5]. Using this representation, the function maximum varies linearly over the (side)slip with changing maximum friction coefficient (cf. dashed black line in **Figure 2**). The function $f_y(\lambda, \mu_{max}, F_z)$ for one set of parameters C, E, c_1, and c_2, constant wheel load F_z and changing maximum friction coefficient μ_{max}, representing dry, wet, and icy conditions can be seen in **Figure 2**.

The function $h(F_{x,y}) = \cos(\arctan(B_{xy}F_{y,x}))$ accounts for the reduced forces in the presence of both lateral and longitudinal forces, with scaling factor B_{xy} [15]. Furthermore, the lateral forces F_y are modeled as PT_1-element as

$$F_y + \frac{l_t}{v_{t,x}}\dot{F}_y = f_y(\alpha, \mu_{max}, F_z)h(F_x), \tag{6}$$

with tire-delay constant l_t [16].

http://dx.doi.org/10.5772/intechopen.71900

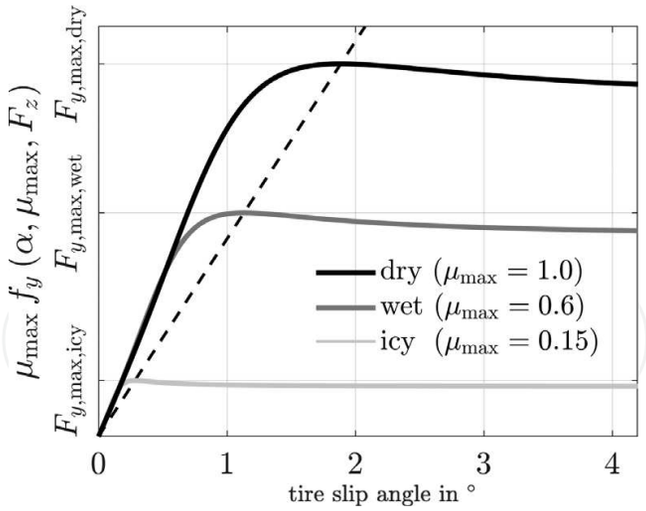

Figure 2. Schematic visualization of the used vehicle dynamics model.

The inputs to the system are the drive and break torques M_d and M_b, and the steering angle δ (cf. **Figure 3**). This leads to the equation of motion for the rotational velocity of one tire ω_t

$$J_\text{t}\dot{\omega}_\text{t} = M_\text{d} - M_\text{b} - M_\text{res} - F_x r_\text{t}, \tag{7}$$

with the tire's moment of inertia J_t, and a moment due to rolling resistance

$$M_\text{res} = F_z(c_{\text{res},1} + c_{\text{res},2}\omega_\text{t}), \tag{8}$$

with constant and velocity dependent part, represented by $c_{\text{res},1}$ and $c_{\text{res},2}$, respectively.

2.2. Vehicle body dynamics

Considering a two-track model with additional roll dynamics as displayed in **Figures 1** and **4**, the vehicle's dynamics under disregard of vertical dynamics can be described by the vehicle's yaw-rate $\dot{\psi}$, its sideslip angle β, the roll angle and rate κ and $\dot{\kappa}$, and its center of gravity (c.o.g.)

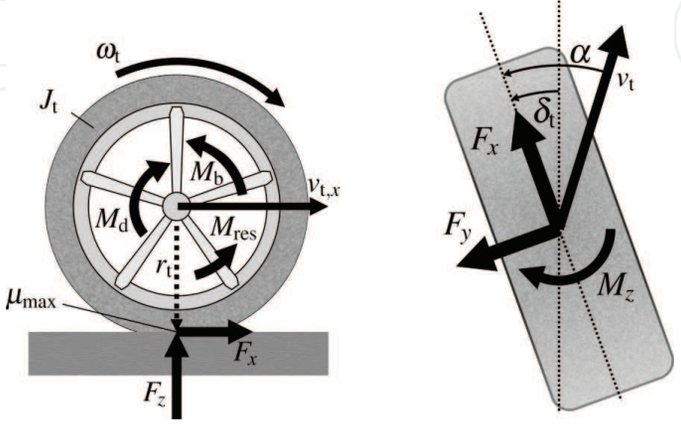

Figure 3. Torques and forces acting on the tire.

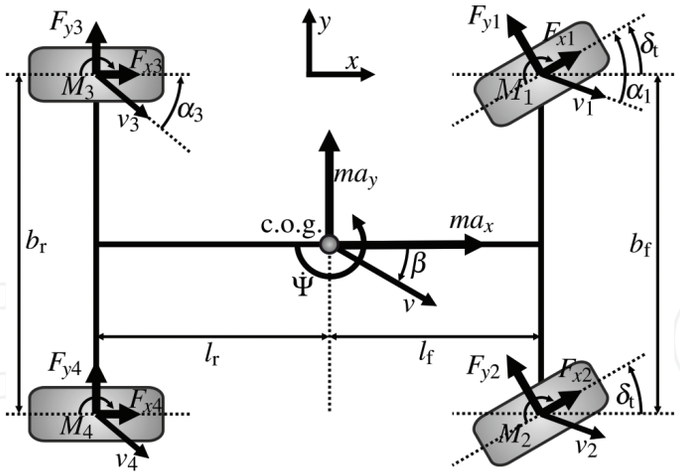

Figure 4. Top view of a two-track model including geometrical parameters.

velocity v. These quantities represent the angular velocity of rotation around the vertical axis, the angle between the vehicle's longitudinal axis and its velocity vector, the angle and rate between the vehicle's vertical axis and the stationary vertical axis, and the velocity of the center of gravity, respectively. This leads to the following equations of motion

$$J_z\ddot{\psi} = l_\mathrm{f}\left(F_{y1} + F_{y2}\right)\cos\left(\delta_\mathrm{t}\right) - l_\mathrm{r}\left(F_{y3} + F_{y4}\right) - \sum_{i=1}^{4} M_{z,i}, \tag{9}$$

$$mv\left(\dot{\beta} + \dot{\psi}\right) = \left(F_{y1} + F_{y2}\right)\cos\left(\beta - \delta_\mathrm{t}\right) + \left(F_{y3} + F_{y4}\right)\cos\left(\beta\right), \tag{10}$$

$$m\dot{v} = \left(F_{x1} + F_{x2}\right)\cos\left(\beta - \delta_\mathrm{t}\right) + \left(F_{x3} + F_{x4}\right)\cos\left(\beta\right) - F_\mathrm{air}, \tag{11}$$

$$m_\mathrm{a}h_\mathrm{r}a_\mathrm{y} = J_\kappa\ddot{\kappa} + d_\kappa(\dot{\kappa}) - c_\kappa(\kappa) - m_\mathrm{a}gh_\mathrm{r}\sin\kappa, \tag{12}$$

with l_f, l_r being the distance between front and rear axes to the c.o.g., respectively, mass m being moment of inertia with respect to the vertical axis J_z, velocity and acceleration of the c.o.g. v, $\dot{v}$, forces due to air resistance F_air, and self-aligning torques $M_{z,i}$.

Roll dynamics are represented in analogy to a spring-damper system with gravitational influence with chassis mass m_a, distance between roll axis and c.o.g. h_r, moment of inertia with respect to the roll axis J_κ, gravitational acceleration g, and nonlinear spring and damper coefficients $c_\kappa(\kappa)$ and $d\dot{\kappa}(\dot{\kappa})$, respectively. These characteristics are represented by

$$c_\kappa(\kappa) = c_{\kappa,1}\kappa + c_{\kappa,2}\kappa^3, \tag{13}$$

$$d_{\dot{\kappa}}(\dot{\kappa}) = d_{\dot{\kappa},1}\dot{\kappa} + d_{\dot{\kappa},2}\tanh(\dot{\kappa}). \tag{14}$$

These constants result from combinations of suspension and stabilization constants $c_{\mathrm{f,r}}$, $d_{\mathrm{f,r}}$, and $c_{\mathrm{st,f,r}}$, respectively (cf. **Figure 1**). In conclusion, the resulting system state vector can be expressed as

$$\boldsymbol{x} = \left[\dot{\psi}, \beta, \kappa, \dot{\kappa}, F_{y,i}, \omega_i, v\right]^\mathrm{T}. \tag{15}$$

2.3. Measurement model

Inside the vehicle, standard sensors are implemented to obtain information about the current driving state. These sensors measure the yaw-rate $\dot{\psi}$, longitudinal and lateral acceleration $a_{x,\mathrm{s}}$ and $a_{y,\mathrm{s}}$, and the four rotational velocities of the vehicle's tires ω_i. This leads to the measurement vector

$$y = \left[\dot{\psi}, a_{x,\mathrm{s}}, a_{y,\mathrm{s}}, \omega_{\mathrm{t},i}\right]^{\mathrm{T}}. \tag{16}$$

A measurement model representing these sensors is needed for the later implementation of KF derivatives. Since the measured yaw-rate and wheel velocities are states within the model, they are obtained directly and no further model is needed. The longitudinal and lateral accelerations in the sensor position $a_{x,\mathrm{s}}$ and $a_{y,\mathrm{s}}$, respectively, can be described by

$$a_{x,\mathrm{s}} = \dot{v}\,\cos\beta - v\left(\dot{\beta}+\dot{\psi}\right)\sin\beta - l_y\ddot{\psi} + \dot{\psi}\left(l_z\dot{\kappa} - l_x\dot{\psi}\right), \tag{17}$$

$$a_{y,\mathrm{s}} = \dot{v}\,\sin\beta + v\left(\dot{\beta}+\dot{\psi}\right)\cos\beta - l_z\ddot{\kappa} + l_x\ddot{\psi} - l_y\dot{\kappa}^2 - l_y\dot{\psi}^2, \tag{18}$$

with l_x, l_y, and l_z being the components of the distances from the c.o.g. to the sensor position.

Due to the sensors' sampling rate of 100 Hz, all later implementations on the control unit will be running at this frequency. Therefore, the continuous time differential Eqs. (1)–(18) are discretized using first-order Euler discretization.

Within the model, numerous parameters are utilized. These parameters can either be measured directly, e.g., geometrical parameters, or need to be identified using an offline identification algorithm. Since the model is strongly nonlinear, a particle swarm algorithm (PSO) is used. Therefore, measurements representing longitudinal and lateral dynamics, driven by a test vehicle, have to be performed. Hence, a sequential identification can be realized, first considering longitudinal excitation, neglecting lateral dynamics and subsequently lateral excitation. Further details can be found in Ref. [15].

In summary, the vehicle's dynamics can be expressed by the discrete time state space representation

$$\boldsymbol{x}_{k+1} = \boldsymbol{f}(\boldsymbol{x}_k, \boldsymbol{u}_k; \boldsymbol{p}), \tag{19}$$

$$\boldsymbol{y}_{k+1} = \boldsymbol{g}(\boldsymbol{x}_{k+1}, \boldsymbol{u}_{k+1}; \boldsymbol{p}), \tag{20}$$

at discrete time step $\boldsymbol{k}$ with all parameters included in $\boldsymbol{p}$. Thereby, $\boldsymbol{x} \in \mathbb{R}^{\mathbf{13}\times\mathbf{1}}$ represents the system state and $\boldsymbol{y} \in \mathbb{R}^{\mathbf{7}\times\mathbf{1}}$ represents the measurement vector.

3. State and parameter estimation

In this section, a brief overview over the used Kalman filter derivative will be given. At first, the algorithm for state estimation will be presented. Furthermore, a model-based dead-time

compensation will be introduced. Secondly, the joint UKF for state and parameter estimation will be presented. Subsequently, an extension for the estimation of bounded parameters is introduced.

3.1. The unscented Kalman filter for state estimation

The process and measurement model presented in Section 2 are strongly nonlinear, especially considering the forces acting on the vehicle's tires (cf. Eq. (5)). Therefore, a Kalman filter derivative, capable of estimating nonlinear systems, the UKF is utilized. Since no information about the covariance is available, the additive form of the process and measurement equations

$$\boldsymbol{x}_{k+1} = \boldsymbol{f}(\boldsymbol{x}_k, \boldsymbol{u}_k; \boldsymbol{p}) + \boldsymbol{w}_k, \tag{21}$$

$$\boldsymbol{y}_{k+1} = \boldsymbol{g}(\boldsymbol{x}_{k+1}, \boldsymbol{u}_{k+1}; \boldsymbol{p}) + \boldsymbol{v}_{k+1}, \tag{22}$$

with $\boldsymbol{w}_k \propto \mathcal{N}(\boldsymbol{0}, \boldsymbol{Q})$, $\boldsymbol{Q} \in \mathbb{R}^{n_x \times n_x}$ and $\boldsymbol{v}_k \propto \mathcal{N}(\boldsymbol{0}, \boldsymbol{R})$, $\boldsymbol{R} \in \mathbb{R}^{n_y \times n_y}$ representing the process and measurement uncertainties by uncorrelated Gaussian random numbers, is assumed. The system state and measurement are described by the state and measurement vectors $\boldsymbol{x}_k \in \mathbb{R}^{n_x}$ and $\boldsymbol{y}_k \in \mathbb{R}^{n_y}$ with state dimension n_x and measurement dimension n_y. To initialize the filter, initial values for the state and covariance estimation, $\widehat{x}_0 \in \mathbb{R}^{n_x}$ and $\widehat{P}_0 \in \mathbb{R}^{n_x \times n_x}$, respectively, have to be set. Following this, the recursive estimation divided in two steps, i.e., the process and measurement update can be realized. Within the process update, an *a priori* state and covariance estimation utilizing the process model is executed. Using the unscented transformation [17], a carefully chosen set of $2n_x + 1$ sigma points for time step $k \in \{0, \ldots, \infty\}$

$$x_{k,0} = \widehat{x}_k, \tag{23}$$

$$x_{k,i} = \widehat{x}_k + \left(\sqrt{(n + \lambda_{\text{ukf}})\widehat{P}_k}\right)_i \quad \text{for} \quad i = 1, \ldots, n_x, \tag{24}$$

$$x_{k,i} = \widehat{x}_k - \left(\sqrt{(n + \lambda_{\text{ukf}})\widehat{P}_k}\right)_{i-n_x} \quad \text{for} \quad i = i + 1, \ldots, 2n_x, \tag{25}$$

with $\widehat{x}_k$ and $\widehat{P}_k$ representing the current state and covariance estimation, respectively, are calculated. Thereby, $\lambda_{\text{ukf}} = \alpha_{\text{ukf}} n_x + \kappa_{\text{ukf}} - n_x$, with scaling parameters α_{ukf} and κ_{ukf}. Furthermore, $\left(\sqrt{(n + \lambda_{\text{ukf}})\widehat{P}_k}\right)_i$ is the ith column of the matrix square root, e.g., using Cholesky decomposition. These sigma points characterize the current probability density function and undergo the real nonlinear transformation utilizing Eq. (21) to calculate the *a priori* estimation as

$$\boldsymbol{x}^-_{k+1,i} = \boldsymbol{f}(\boldsymbol{x}_{k,i}, \boldsymbol{u}_k; \boldsymbol{p}), \tag{26}$$

$$\boldsymbol{x}^-_{k+1} = \sum\nolimits_{i=0}^{2n_x} W_i^{\text{m}} \boldsymbol{x}^-_{k+1,i}, \tag{27}$$

$$\boldsymbol{P}^-_k - = \sum\nolimits_{i=0}^{2n_x} W_i^{\text{c}} \left(\boldsymbol{x}^-_{k+1,i} - \boldsymbol{x}^-_{k+1}\right)\left(\boldsymbol{x}^-_{k+1,i} - \boldsymbol{x}^-_{k+1}\right)^{\text{T}}, \tag{28}$$

$$\boldsymbol{y}_{k+1,i}^{-} = \boldsymbol{h}(\boldsymbol{x}_{k+1,i}, \boldsymbol{u}_{k+1}; \boldsymbol{p}), \tag{29}$$

$$\boldsymbol{y}_{k+1}^{-} = \sum\nolimits_{i=0}^{2n_x} W_i^{\mathrm{m}} \boldsymbol{y}_{k+1,i}^{-}. \tag{30}$$

Following this, a measurement $\boldsymbol{y}_{k+1}$ is received and the measurement update

$$P_{xy,k+1} = \sum\nolimits_{i=0}^{2n_x} W_i^{\mathrm{c}} \left(\boldsymbol{x}_{k+1,i}^{-} - \boldsymbol{x}_{k+1}^{-}\right)\left(\boldsymbol{y}_{k+1,i}^{-} - \boldsymbol{y}_{k+1}^{-}\right)^{\mathrm{T}}, \tag{31}$$

$$P_{yy,k+1} = \sum\nolimits_{i=0}^{2n_x} W_i^{\mathrm{c}} \left(\boldsymbol{x}_{k+1,i}^{-} - \boldsymbol{x}_{k+1}^{-}\right)\left(\boldsymbol{y}_{k+1,i}^{-} - \boldsymbol{y}_{k+1}^{-}\right)^{\mathrm{T}}, \tag{32}$$

$$\boldsymbol{K}_{k+1} = \boldsymbol{P}_{xy,k+1}\boldsymbol{P}_{yy,k+1,}^{-1} \tag{33}$$

$$\widehat{\boldsymbol{x}}_{k+1} = \boldsymbol{x}_{k+1}^{-} + \boldsymbol{K}_{k+1}\left(\boldsymbol{y}_{k+1} - \boldsymbol{y}_{k+1}^{-}\right), \tag{34}$$

$$\widehat{\boldsymbol{P}}_{k+1} = \boldsymbol{P}_{k+1}^{-} - K_{k+1}P_{yy,k+1}K_{k+1}^{\mathrm{T}}, \tag{35}$$

with weighting factors $W_i^{\mathrm{m,c}}$ can be executed. This leads to the *a posteriori* estimations of the state and covariance, $\widehat{\boldsymbol{x}}_{k+1}$ and $\widehat{\boldsymbol{P}}_{k+1}$, respectively [18].

3.2. Dead-time compensation

When designing online methods for real-time applications, dead times are frequently to face. Especially, considering vehicular applications, the communication is realized via CAN-Bus, leading to dead times. In the following, a method to compensate for dead times within state estimation is presented.

Since the measurement update (Eqs. (31)–(35)) can only be processed, as soon as a measurement y_k is received, dead times t_{d} corrupt the UKF severely. Ignoring this dead time may lead to poor filter performance or even divergence. One solution is to accept the dead time and delay the estimation by exact this time. Alternatively, the system's state and covariance can be estimated by performing the process update (Eqs. (26)–(28)) during the dead time without doing the measurement update, based on the delayed filter estimation up to time step k, so that the state estimation at discrete time step $k + n_{t_{\mathrm{d}}}$, where $n_{t_{\mathrm{d}}}$ is the number of discrete time steps due to the dead time is

for j = 1 to $n_{t_{\mathrm{d}}}$ do

$$\boldsymbol{x}_{k+j-1,0} = \widehat{\boldsymbol{x}}_{k+j-1} \tag{36}$$

$$\boldsymbol{x}_{k+j-1,i} = \widehat{\boldsymbol{x}}_{k+j-1} + \left(\sqrt{(n+\lambda_{\mathrm{ukf}})\widehat{\boldsymbol{P}}}_{k+j-1}\right)_i \text{ for } i = 1, \ldots, n_x \tag{37}$$

$$\boldsymbol{x}_{k+j-1,i} = \widehat{\boldsymbol{x}}_{k+j-1} - \left(\sqrt{(n+\lambda_{\mathrm{ukf}})\widehat{\boldsymbol{P}}}_{k+j-1}\right)_{i-n_x} \text{ for } i = i+1, \ldots, 2n_x \tag{38}$$

$$\boldsymbol{x}_{k+j,i}^{-} = \boldsymbol{f}\left(\boldsymbol{x}_{k+j-1}, \boldsymbol{u}_{k-1}; \boldsymbol{p}\right) \tag{39}$$

$$\widehat{\boldsymbol{x}}_{k+j} = \sum_{i=0}^{2n_x} W_i^{\mathrm{m}} x_{k++j,\,i}^{-} \tag{40}$$

$$\widehat{\boldsymbol{P}}_{k+j} = \sum_{i=0}^{2n_x} W_i^{\mathrm{c}} \left(\boldsymbol{x}_{k+j,\,i}^{-} - \widehat{\boldsymbol{x}}_{k+j}\right)\left(\boldsymbol{x}_{k+j,\,i}^{-} - \widehat{\boldsymbol{x}}_{k+j}\right)^{\mathrm{T}} \tag{41}$$

end

To reduce computational cost, the update steps can be reduced, so that only the mean is transformed and therefore no further sigma point needs to be calculated and transformed as

for j=1 to n_{t_d} do

$$\widehat{\boldsymbol{x}}_{k+j} = \boldsymbol{f}\left(\widehat{\boldsymbol{x}}_{k+j-1}, \boldsymbol{u}_{k-1}; \boldsymbol{p}\right) \tag{42}$$

end

This may lead to reduced performance, depending on the length of the dead time, the process model complexity, and the uncertainties within the process.

3.3. Parameter estimation

Since parameters may vary within dynamic systems, simultaneous state and parameter estimation is considered. Various methods to solve this task have been developed in the past decades. In the following, the approach of joint state and parameter estimation is presented. Therefore, states and parameters are concentrated into one joint state vector as

$$x_k = \begin{bmatrix} \boldsymbol{x}_k \\ \boldsymbol{p}_{\mathrm{est},\,k} \end{bmatrix}, \tag{43}$$

with primary state $\boldsymbol{x}_k \in \mathbb{R}^{n_x}$ and parameters to be estimated $\boldsymbol{p}_{\mathrm{est},\,k} \in \mathbb{R}^{n_p}$. The model within the process update assumes constant parameters, i.e., $\boldsymbol{p}_{\mathrm{est},\,k+1} = \boldsymbol{p}_{\mathrm{est},\,k}$. The remaining UKF algorithm stays the same, with only the dimension of the estimated state $\widehat{\tilde{\boldsymbol{x}}}_k \in \mathbb{R}^{n_x+n_p}$ changing.

If some parameters are bounded as $a_i \leq \boldsymbol{p}_{\mathrm{est},\,i} \leq b_i$, these are not estimated directly, but using a substitute parameter $\boldsymbol{p}_{\mathrm{sub},\,i}$ as

$$\boldsymbol{p}_{\mathrm{est},\,i} = \frac{b_i - a_i}{2} \tanh\left(\boldsymbol{p}_{\mathrm{sub},\,i}\right) + \frac{a_i + b_i}{2}. \tag{44}$$

Using this substitution, the estimated parameter $\boldsymbol{p}_{\mathrm{sub},\,i}$ is not bounded and leads to the real parameters for $\boldsymbol{p}_{\mathrm{est},\,i}$ in the intended range.

4. Estimation results

In this section, the results of the vehicle's states and parameter estimation using an unscented Kalman filter and the two-track model described Section 2 are presented. At

first, the test vehicle and the measurement equipment that is necessary for the validation are introduced. Secondly, the results of the vehicle state estimation and the results by considering dead time within the estimation are shown. Furthermore, a simultaneous state and friction estimation are presented that exhibit improved estimation results for varying road conditions.

4.1. Measurement setup

The estimation results are verified by using a Volkswagen Golf GTE Plug-In Hybrid (**Figure 5(a)**) equipped with a Genesys ADMA-G-Eco + (**Figure 5(b)**). This system is developed especially for vehicle dynamics testing in the automotive sector. This inertial measurement unit (IMU) corrected by global positioning system (GPS) enables precise measurement of acceleration, speed, and position of the moving test vehicle in all three-dimensional axes. Furthermore, the pitch, roll and yaw angles, angular velocities as well as sideslip angle can be obtained. The GPS antenna is mounted on the roof of the test vehicle, whereas the IMU is placed in the footwell of the passenger seat. Ideally, the two sensors are placed in the center of gravity; unfortunately, in praxis, this requirement usually either cannot or can only be fulfilled with very high effort. Furthermore, it is hardly possible to exactly align the ADMA's measurement axes with the vehicle's axes. The errors caused by the distance between the installation position and the c.o.g as well as by misalignment angle can be mathematically compensated considering the lever arms and the angle offsets, respectively. The IMU's measurements are exclusively provided for the validation of the Kalman filter application. Additional measurements of the wheel speeds, accelerations and yaw rate as well as system inputs, i.e., steering angle, engine, and breaking torque, are taken from the vehicle's bus system. The onboard measurements are provided for the measurement update of the real-time Kalman filter application. Furthermore, an ES910 prototyping and interface module provides the connection to the vehicle bus and the computation of the filter application with system-level behavior.

4.2. Unscented Kalman filter setup

The UKF utilizes a two-track model including roll dynamics as described in Section 2. The estimator's state and measurement vector were therefore

(a) Volkswagen Golf GTE plug-in-Hybrid (b) Measurement setup

Figure 5. Test vehicle and measurement equipment.

$$\boldsymbol{x} = \left(\dot{\psi}, \beta, \kappa, \dot{\kappa}, F_{y_i}, \omega_i, v_{\text{cog}}\right)^{\text{T}}, \tag{45}$$

$$\boldsymbol{y} = \left(\dot{\psi}, a_{y,\text{s}}, a_{x,\text{s}}, \omega_i\right)^{\text{T}}. \tag{46}$$

α_{UKF} determines the spread of the sigma points around the mean $\hat{\boldsymbol{x}}$ and is set to 1, the scaling parameter κ_{UKF} is usually set to 0, and $\beta_{\text{UKF}} = 2$ is an optimal value to approximate distribution of $\boldsymbol{x}$ as Gaussian distribution. The process and measurement covariances are empirically determined and set up to

$$\boldsymbol{Q} = \text{diag}\left(10^4, 1, 1, 1, 1, 1, 1, 1, 1, 10^{10}, 10^{10}, 10^{10}, 10^{10}, 1\right)10^{-15} \tag{47}$$

$$\boldsymbol{R} = \text{diag}\left(10^{-6}, 10^{-3}, 10^{-2}, 10^{-3}, 10^{-3}, 10^{-3}, 10^{-3}\right). \tag{48}$$

The initial covariance matrix of the state distribution is initialized with $\boldsymbol{P}_0 = \boldsymbol{Q}$.

4.3. State estimation

In this section, the results of vehicle state estimation are shown. The UKF estimation results are displayed in light grey, while the reference measurements of the ADMA-G-Eco +are displayed in black and the vehicle`s onboard measurements are displayed in grey. Each displayed maneuver is subdivided into eight diagrams. The top line shows yaw-rate and sideslip angle representing lateral dynamics, and the second line shows roll angle and roll rate representing roll dynamics. Furthermore, the velocity in the c.o.g. and the wheel speeds representing longitudinal dynamics are displayed in the third line and at last longitudinal and lateral acceleration in the bottom line. The accelerations in the c.o.g are displayed with continuous lines and the accelerations measured with onboard acceleration sensor that is not mounted in the c.o.g. in the dashed lines. The distances of the sensor position from the c.o.g. are identified with $l_x = 1.07$ m, $l_y = -0.39$ m, and $l_z = 0.55$ m. In order to demonstrate the estimation quality, **Figure 6** shows a steering sweep maneuver with periodical steering angle input at nearly constant amplitude and increasing frequency and at a constant velocity of 37 km/h Despite the varying frequency, an accurate estimation of all dynamic states is evident, accompanied by improved estimation of the vehicles velocity compared to the onboard measurement of the vehicles' velocity. Only for the roll angle, a higher deviation can be recognized. This results from varying lateral inclination of the test road.

A steering sweep maneuver is optimal to validate the filter application and the integrated vehicle dynamic models, but it is not a practical example, whereas, for example, lane change maneuvers often occur. In addition, lane change maneuvers enable high lateral acceleration and high values of tire sideslip angles, which may lead, under certain conditions, to loss of stability due to nonlinear tire characteristics. Therefore, lane change maneuvers are suitable as practical driving situation.

http://dx.doi.org/10.5772/intechopen.71900

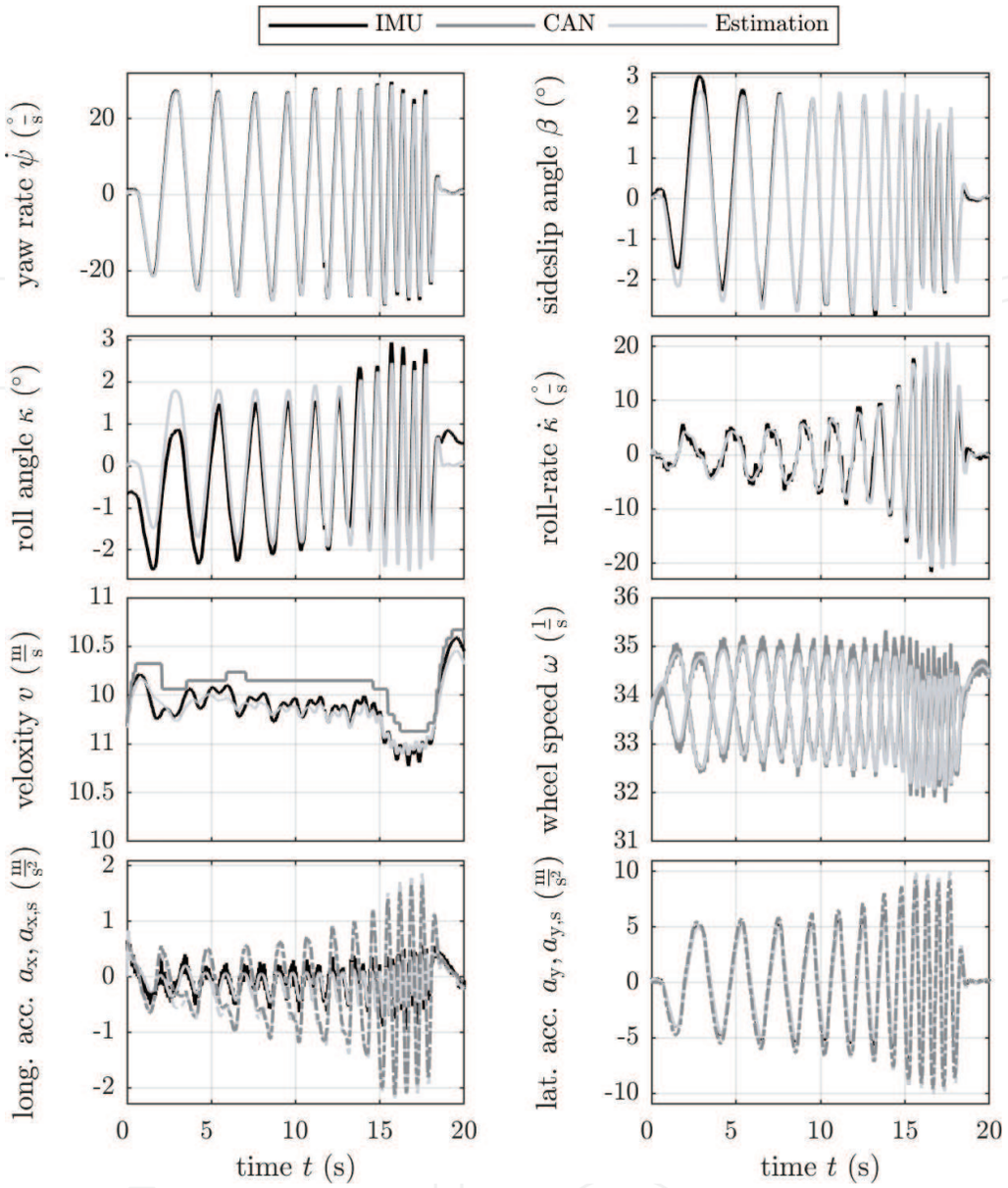

Figure 6. Vehicle state estimation during steering sweep maneuver.

A double-lane change maneuver with moderate lateral acceleration represents a typical maneuver on highways or freeways occurring by overtaking another slower moving vehicle. However, a double-lane change maneuver with high lateral acceleration represents obstacle avoidance maneuver. This kind of maneuver is displayed with a high lateral acceleration up to $a_y = 7\ \mathrm{m/s^2}$ and with nearly constant velocity of $v = 37\,\mathrm{km/h}$ in **Figure 7**. It can be stated that also an accurate estimation of all relevant states can be seen over the whole maneuver, and again particularly an improved velocity estimation compared to onboard measurement can be emphasized. The higher estimation performance of the velocity can be advantageous for some control applications, such as collision avoidance.

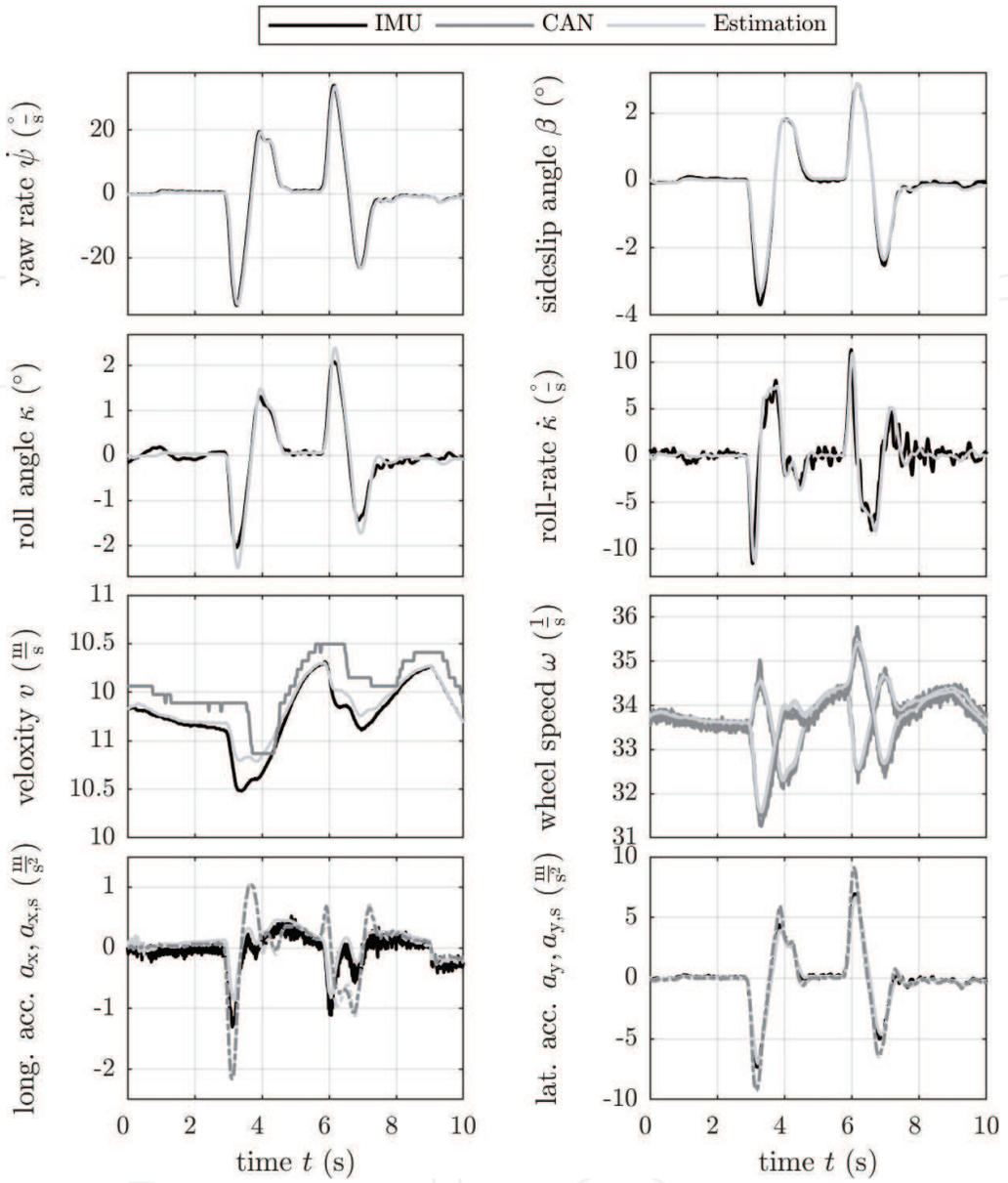

Figure 7. Vehicle state estimation during double-lane change maneuver.

4.4. Dead-time compensation

A major problem in control systems is dead time. Dead time may lead either to poor control results or to unstable control. In case of stability control systems and therefore for robust car steering, the real-time information of sideslip angle and yaw rate is very important. As pointed previously, an accurate estimation of this vehicle states can be realized using UKF with nonlinear two-track model even if vehicles move at its stability limits. However, the estimated states are not the true vehicle states at this particular time. They are delayed due to the dead-time-shifted measurement update, which occurs particularly of the communication on the CAN network. In dependence on the length of dead time, different arrangements exist for dead-time compensation. In addition, to consider

the dead time in the controller designing, a further possibility is model-based dead-time compensation within state estimation. A simple method to predict the system's state and covariance during the dead time is to execute only the filter process update without doing the measurement update as defined in Section 3.2. Alternatively, to reduce computational cost, the prediction can be executed only considering the mean of the system states by neglecting further sigma points. During the prediction from time step k to $k + n_{t_d}$, there are no further information of the system input. Therefore, the last known system input is used for the prediction. From this follows a prediction error that decreases with less dynamics of the system input. A comparison of both possibilities and the quality of the dead-time compensation within the vehicle state estimation is shown in **Figure 8**. A step steering maneuver on dry asphalt at a velocity of approximately 50 km/h with maximum lateral acceleration of almost $a_y = 7\,\mathrm{m}/s^2$ is considered. The top diagram shows the yaw rate and the next diagram the sideslip angle, while measurements are displayed in black, the UKF's state estimation without dead-time compensation in grey, the dead-time compensated state estimation by using all sigma points in dashed light grey, and the dead-time compensated state estimation by using only the mean in dash-dotted grey. In the present case, the predominant dead time amounts about 30 ms that corresponds to $n_{t_d} = 3$. The dead time is determined by comparing redundant measurements that are obtained from the IMU of the ADMA and the vehicle's onboard CAN bus.

It is quite obvious that both methods for dead-time compensation do not really differ in the application of vehicle dynamics; thus, it is at an advantage due to reduced computational costs only to consider the mean of the state. Furthermore, the UKF results with dead-time-compensated

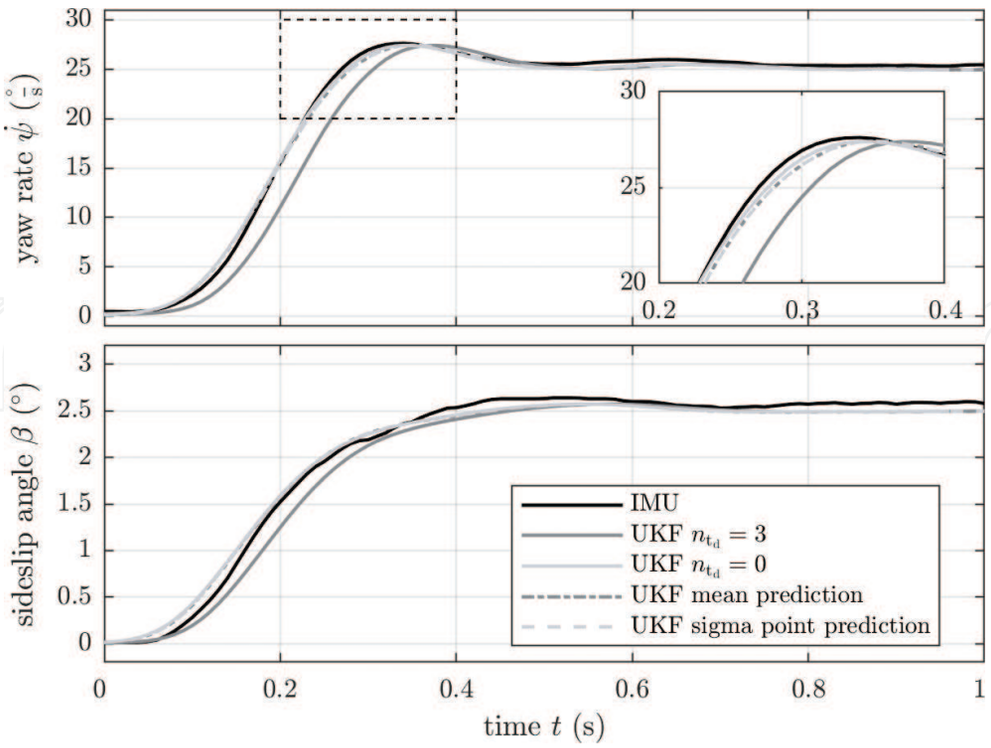

Figure 8. Dead-time-compensated vehicle state estimation during step steering maneuver.

states also do not differ from the time-shifted UKF prediction without dead time displayed in light grey. Therefore, it is possible to include dead-time compensation in the state estimation in a simple manner and to obtain precise estimation results. However, this method for dead-time compensation has the restriction that the system does not contain varying dead time and the dead time is well known.

All previously presented test maneuvers are executed on dry asphalt. Thus, the maximum friction coefficient between road and tire is well known. Under different road conditions, for example, wet, snow, and ice and without adaption of the friction coefficient, the accuracy of the state estimation decreases highly. Hence, for precise state estimation, it is essential to estimate the maximum friction coefficient as well.

4.5. Maximum friction coefficient estimation

However, not only for improved vehicle state estimation a simultaneous estimation of the maximum friction coefficient between road and tire is of paricular importance. To ensure a proper functionality of safety functions not only the knowledge of the driving situation but also of the driving environment, in particular the road condition, is required. This section focuses on the road condition classification using a joint unscented Kalman filter approach as described in Section 3.3. The extended process, covariance matrix $\boldsymbol{Q}_{\mathrm{p}}$, for the maximum friction coefficient estimation is empirically determined and set up to

$$\boldsymbol{Q}_{\mathrm{p}} = \mathrm{diag}\big(\mathrm{diag}(\boldsymbol{Q}), 10^{-8}\big). \tag{49}$$

Furthermore, the maximum friction coefficient is bounded according to Eq. (37) with a upper bound of 1.1 and a lower bound of 0.1. The upper bound corresponds to the best traction potential that may occur when the roads are dry and the tires are in good condition. The lower bound corresponds to the lowest traction potential that may occur when the roads are icy and the tires have a low tire profile.

In **Figure 9**, again a double-lane change maneuver on dry asphalt at a velocity of approximately 43 km/h with maximum lateral acceleration of almost $a_{\mathrm{y}} = 9\ \mathrm{m/s^2}$ is considered. The top diagram shows the measured system input namely the steering angle. The following diagrams show the yaw rate, the lateral acceleration, and the sideslip angle, while the IMU's measurements are displayed in black and the onboard measurements in grey, and the UKF's estimations in light grey. The bottom diagram shows the estimated maximum friction coefficient, while the initial value is wrongly set to $\mu_{\max} = 0.4$. By using offline identification algorithms, the reference value for the maximum friction coefficient was determined at approximately 1. The light red lines show the state estimation without adaptation of friction coefficient. Obviously, an accurate sideslip and yaw-rate estimation can only be guaranteed with adaptation of the friction coefficient. However, an adaption of the friction coefficient is only possible during phases of sufficient excitation. At the beginning and at the end of the maneuver without steering, no adaption may take place.

http://dx.doi.org/10.5772/intechopen.71900

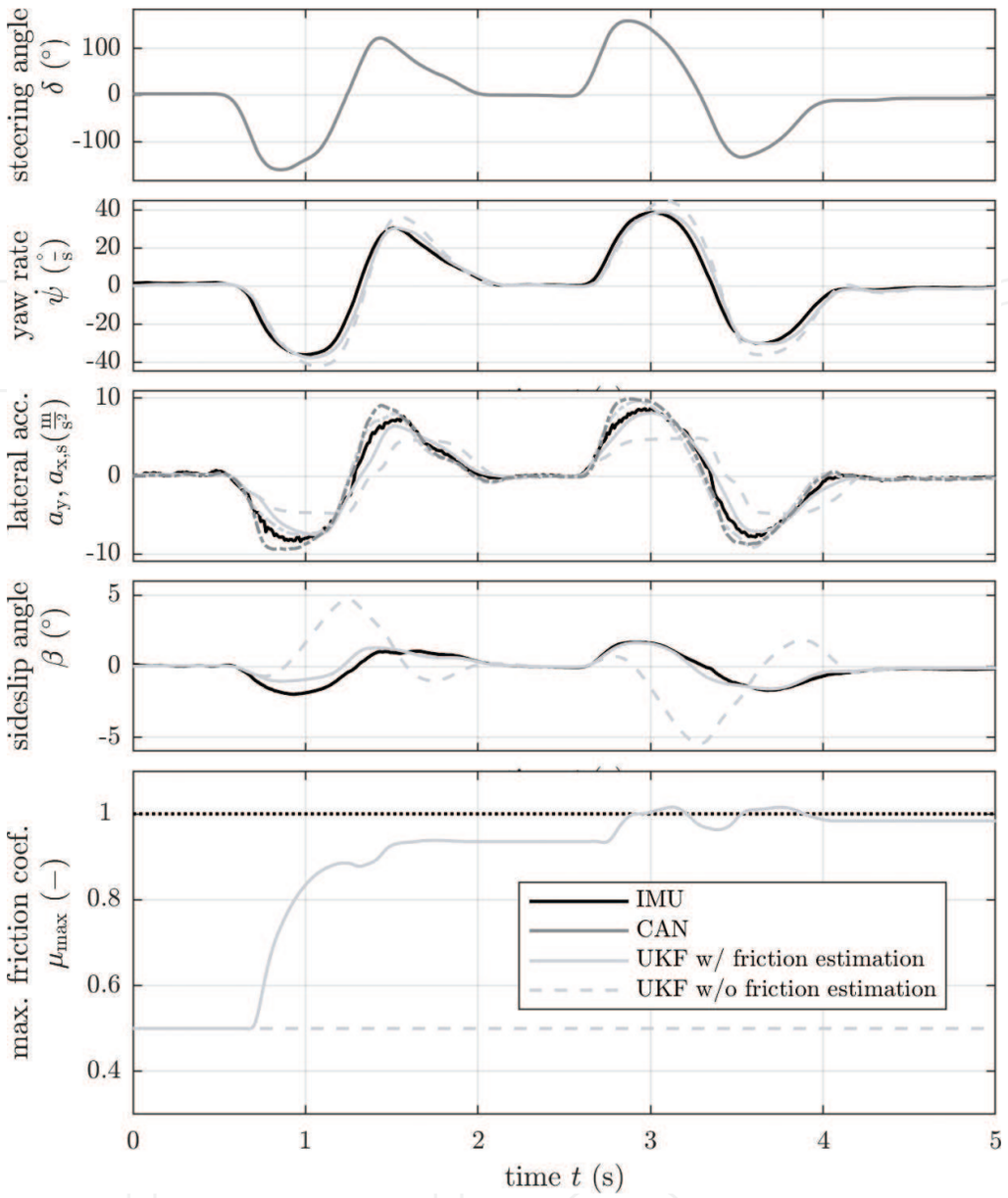

Figure 9. Vehicle state and maximum friction coefficient estimation during double-lane change maneuver on dry asphalt.

When sufficient excitation exists, the maximum friction coefficient can be estimated within few seconds.

In **Figure 10**, the estimation of the maximum friction coefficient on different roads is displayed. Beginning on dry asphalt, the test vehicle drives a sine steering maneuver and changes over to wet steel. Wet steel exhibits similar properties regarding traction potential as an icy road. Because it is much easier to build up a road composed of wet steel than of ice to carry out a test, in this test, the wet steel represents a road with low traction potential. Over the entire period of the sine maneuver, a sufficient excitation is existent. Hence, the unscented Kalman

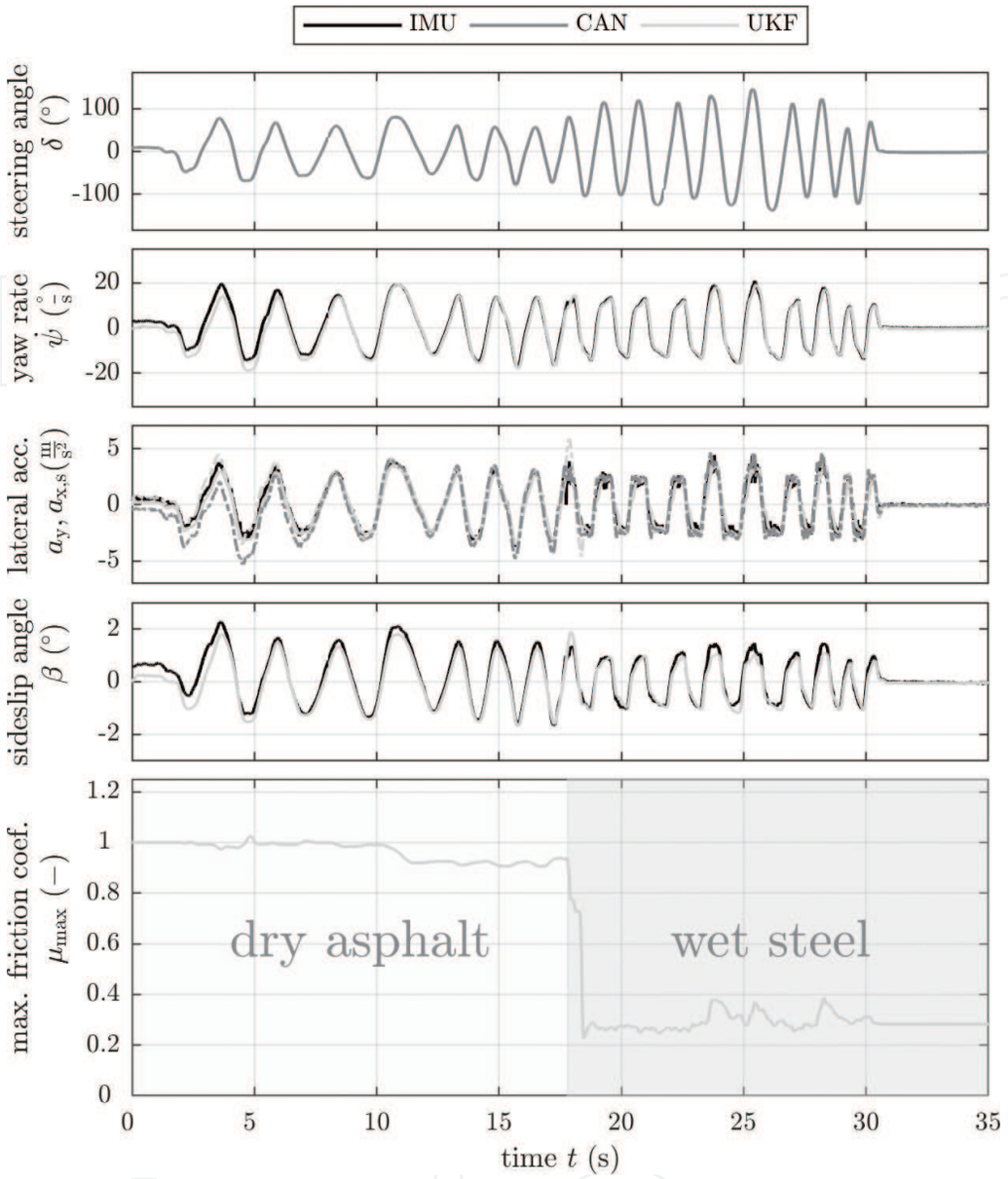

Figure 10. Vehicle state and maximum friction coefficient estimation during sine steering maneuver on dry asphalt and wet steel.

filter estimates while driving over the dry asphalt a maximum friction coefficient of approximately 1. After changing to wet steel, clearly, a lower friction level with a maximum friction coefficient of approximately 0.3 is detected. It can be spotted that while sufficient excitation is existent, different friction levels according to different road conditions can also be clearly recognized. The last 5 s of the maneuver is without steering and acceleration, and the estimated maximum friction coefficient remains constant. Therefore, due to missing excitation, it would not be possible to distinguish between dry asphalt and wet steel. Nonsufficient excitation is a major disadvantage of Kalman filter-based approaches for parameter estimation in general and thus also for friction estimation.

A promising approach to solving this problem is to use further source of information, for example, optical sensors and to do an information fusion, so that disadvantages of one information can be compensated by advantages of other information. Information fusion is the next step for improved friction estimation and current research.

5. Conclusion

In this chapter, state and parameter estimation in vehicle dynamics using the unscented Kalman filter is presented. Therefore, a detailed nonlinear process and measurement model of the vehicle are introduced, representing the vehicle's stability and the measurements taken with standard sensors. Dead times, due to CAN communication, are faced and compensated using model-based prediction. The validation of the introduced methods is realized by using a Volkswagen Golf GTE Plug-In Hybrid for high dynamic test maneuvers, e.g., double-lane change. The estimation results are compared with high-precision measurements using a Genesys ADMA inertial measurement unit. Accurate estimation even in situations with lateral acceleration above 7 m/s^2 can be achieved. Furthermore, real-time estimation, compensated for dead times can be realized using model-based prediction.

The parameter estimation is presented using the example of friction coefficient estimation utilizing the joint unscented Kalman filter. Thus, maneuvers with different excitation on different road surfaces are executed. Again, precise estimation in the presence of sufficient excitation can be shown.

Author details

Mark Wielitzka*, Alexander Busch, Matthias Dagen and Tobias Ortmaier

*Address all correspondence to: mark.wielitzka@imes.uni-hannover.de

Institute of Mechatronic Systems, Leibniz Universität Hannover, Germany

References

[1] Best MC, Gordon TJ, Dixon PJ. An extended adaptive Kalman filter for real-time state estimation of vehicle handling dynamics. Vehicle System Dynamics. 2000;**34**(1):57-75. DOI: 10.1076/0042-3114(200008)34:1;1-K;FT057

[2] Cheli F, Sabbioni E, Pesce M, Melzi S. A methodology for vehicle sideslip angle identification: Comparison with experimental data. Vehicle System Dynamics. 2007;**45**(6):549-563. DOI: 10.1080/00423110601059112

[3] Chen BC, Hsieh F-C. Sideslip angle estimation using extended Kalman filter. Vehicle System Dynamics. 2009;**46**(S1):353-364. DOI: 10.1080/00423110801958550

[4] Doumiati M, Victorino AC, Charara A, Lechner D. Onboard real-time estimation of vehicle lateral tire–road forces and sideslip angle. IEEE Transactions on Mechatronics. 2011;**16**(4):601-614. DOI: 10.1109/TMECH.2010.2048118

[5] Pacejka HB, Bakker E. The magic formula tire model. Vehicle System Dynamics. 1992;**21** (S1):1-18. DOI: 10.1080/00423119208969994

[6] Li L, Jia G, Ran X, Song J, Wu K. A variable structure extended Kalman filter for vehicle sideslip angle estimation on a low friction road. International Journal of Vehicle Mechanics and Mobility. 2014;**52**(2):280-308. DOI: 10.1080/00423114.2013.877148

[7] Antonov S, Fehn A, Kugi A. Unscented Kalman filter for vehicle state estimation. Vehicle System Dynamics. 2011;**49**(9):1497-1520. DOI: 10.1080/00423114.2010.527994

[8] Wielitzka M, Dagen M, Ortmaier T. State estimation of vehicle's lateral dynamics using unscented Kalman filter. Los Angeles, USA: IEEE 53rd Annual Conference on Decision and Control (CDC); 15-17 December 2014; 2015. pp. 5015-5020

[9] J Dakhlallah J, Glaser S, Mammar S, Sebsadji Y. Tire-Road Forces Estimation Using Extended Kalman Filter and Sideslip Angle Evaluation. Seattle, USA: 2008 American Control Conference (ACC); 11–13 June 2008; 2008. pp. 4597-4602

[10] Wenzel TA, Burnham KJ, Blundell MV, Williams RA. Dual extended Kalman filter for vehicle state and parameter estimation. Vehicle System Dynamics. 2006;**44**(2):153-171. DOI: 10.1080/00423110500385949

[11] Wielitzka M., Dagen M., Ortmaier T.: Joint unscented Kalman filter for state and parameter estimation in vehicle dynamics. Sydney, Australia: IEEE Conference On Control Applications (CCA); 21-23 September 2015. pp. 1945-1950

[12] Ahn C, Peng H, Tseng HE. Robust estimation of road friction coefficient using lateral and longitudinal vehicle dynamics. Vehicle System Dynamics. 2012;**50**(6):961-985. DOI: 10.1080/00423114.2012.659740

[13] Ahn C, Peng H, Tseng HE. Robust estimation of road friction. IEEE Transactions on Control Systems Technology. 2013;**521**(1):1-13. DOI: 10.1109/TCST.2011.2170838

[14] Wielitzka M, Dagen M, Ortmaier T. State and maximum friction coefficient estimation in vehicle dynamics using UKF. Seattle, USA: American Control Conference (ACC); 24-26 May 2017. pp. 4322-4327

[15] Wielitzka M, Dagen M, Ortmaier T. Nonlinear modeling and parameter identification of Vehicle's lateral dynamics. Tokio, Japan: 12thth International Symposium on Advanced Vehicle Control (AVEC); 22–16 September 2014

[16] Rajamani, Rajesh. Vehicle dynamics and control; Springer Science & Business Media; 2011

[17] Julier SJ. The Scaled Unscented Transformation. 2002: American Control Conference (ACC); 08-10 May 2002. USA: Anchorage; 2012. pp. 4555-4559

[18] Wan EA, Van der Merwe R. The unscented Kalman filter for nonlinear estimation. Alberta, Canada: Adaptive Systems for Signal Processing, Communications, and Control Symposium (AS-SPCC); 04 October 2000. p. 153-158

IntechOpen

IntechOpen